Chapter 6

Iron oxide hydroxide nanoflower assisted removal of arsenic from water

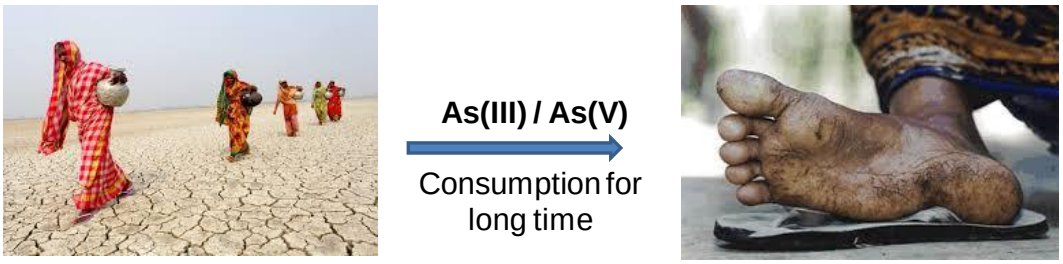

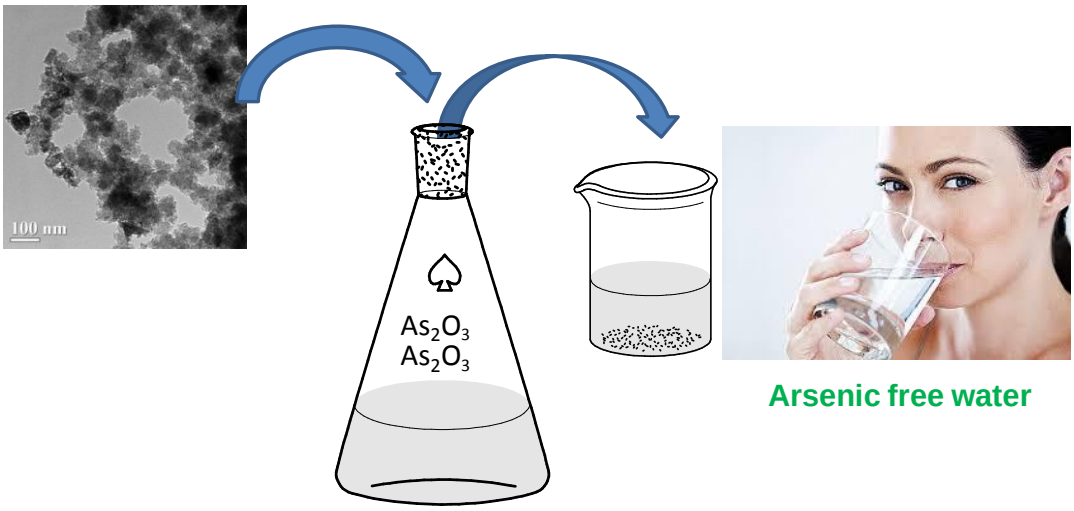

Chapter 6

6.1 Introduction

The occurrence of elevated levels of arsenic in soils and groundwater can compromise soil and water quality and is the reason of major health concerns in humans. Throughout the world, arsenic is creating potentially serious environmental problems for humans and other living organisms. Arsenic is ubiquitous in the earth's crust and is highest in marine shale materials, magmatic sulfides, and iron ores where arsenic occurs as arsenopyrite (FeAsS), realgar (AsS), and orpiment (As_2S_3).[1,2] Oxidative weathering and dissolution of As-containing minerals form dissolved inorganic As(III) and As(V) that are transported in surface or groundwater and can become adsorbed on soil and sediment particles.

Arsenic related problems are found in groundwater water supply systems and are caused by natural processes such as mineral weathering and dissolution resulting from a change in the geo-chemical environment to a reductive condition.[3] Human activities such as mining wastes, petroleum refining, sewage sludge, agricultural chemicals, ceramic manufacturing industries and coal fly ash are also responsible for arsenic contamination.[4-7] The World Health Organization (WHO) announced that water containing more than 50 μgL^{-1} of arsenic is unsuitable due to acute and chronic toxicity. Such a higher level of arsenic is capable of causing mortality due to lung, kidney, or bladder cancer. However, millions of people in Western Bengal, Bangladesh and North-Eastern region of India are drinking groundwater from wells having As concentration of 100-500 μgL^{-1}, and many of these people have succumbed to diseases that are caused by the arsenic contamination.[8] Owing to epidemiological evidence linking arsenic and cancer, the safe limit of arsenic in drinking water was reduced from 50 μgL^{-1} to 10 μgL^{-1} in 1993 by WHO.[8-10]

The distribution between dissolved As(III) and As(V) is dependent on redox condition in groundwater.[11-13] Under oxidizing conditions, the predominant species is As(V), which exists as deprotonated oxyanions of arsenic acid[14] ($H_2AsO_4^-$, $HAsO_4^{2-}$ and AsO_4^{3-}). Under mildly reducing conditions (>+100mV), As(III) is thermodynamically stable[14-16] and exists as arsenious acid (H_3AsO_3, $H_2AsO_3^-$ and $HAsO_3^{2-}$).

Parts of this chapter have been published in

Raul, P.K., Devi, R.R., Umlong, I.M., Thakur, A.J, Banerjee, S., & Veer, V. *Materials Research Bulletin*, **49**, 360--368, 2014.

Recently, it has been recognized that As(III) is more prevalent in groundwater than was previously understood which is of concern because its higher toxicity in comparison to that of As(V).[17] In addition, As(III) is a neutral, uncharged molecule (H_3AsO_3, pKa 9.2) at the pH of most natural water sources[13] and is more mobile because it is less strongly adsorbed on most mineral surfaces than the negatively charged As(V) oxyanions.[18]

A good numbers of works have been reported on removal of As(III) and As(V) from water using nanostructered material with high effiviency.[19-23] But a few studies have investigated the adsorption of As(III) on iron oxide hydroxide materials.[6,24] In this study, following our earlier work we have attempted to prepare iron oxide hydroxide NPs through facile way as NPs are more effective adsorbent compared to their counterpart.[25] The iron oxide hydroxide NPs have several hydroxyl groups which are very effective to bind anions in both ways i.e. covalent bond and hydrogen bond.[26-28] The NPs can be regenerated up to 70% by acid/alkali treatment which certifies its practical application towards dearsenification of water. The behavior of the NPs towards arsenic adsorption was studied varying concentration of arsenic, pH, adsorbent dosage and in presence of different competing anions.

6.2 Experimental Section

6.2.1 Materials

Hydrated ferric sulphate [$Fe_2(SO_4)_3 \cdot xH_2O$] was purchased from Sigma-Aldrich Pvt. Ltd. Urea (NH_2CONH_2), Arsenic(III) oxide (As_2O_3), Sodium hydroxide (NaOH) & Hydrochloric acid (HCl) were purchased from E. Merck (India) Limited, Mumbai. Double distilled water was used throughout the experiments.

6.2.2 Synthesis

The iron oxide hydroxide nanoflower was prepared according to our earlier report.[25] Briefly, 12.5 g (0.1 M) hydrated ferric sulphate [$Fe_2(SO_4)_3 \cdot xH_2O$ (x=5)] was taken in a beaker and dissolved in 250 ml double distilled water. The beaker was placed on a magnetic stirrer and the solution was heated till the temperature of the same attained 60 ^{0}C. The solution was allowed to stir at 60 ^{0}C for 30 minutes, and then 250 ml of 5.0 M urea solution was added drop wise to the solution in the beaker within 3.5 h. During addition of urea to the solution, temperature was maintained at 70 ^{0}C for complete reaction. After complete addition of urea, the solution temperature

was increased to 80 ^{0}C and maintained until the volume of the solution was reduced to the half of the initial volume. Brown precipitate formed after cooling the solution at room temperature (25 ^{0}C). The precipitate was washed repeatedly to remove the alkalinity of the solution and finally oven dried at 70 ^{0}C for 4 h to obtain brown powder, which was taken for subsequent characterization.

6.2.3 Characterization

Phase analysis of iron oxide hydroxide (IOH) NPs was carried out using a X-ray diffractometer (PW 1710, Philips, Holand) with Co Kα radiation (λ = 0.179 nm) with a scanning rate of 3^0 per min. The morphology of the NPs was studied by Field Emission Scanning Electron Microscope (FESEM) instrument (Supra 40, Carl Zeiss) at an accelerating voltage of 20 KV. The particle size of IOH NPs was measured using a Transmission Electron Microscope (TEM) (CM 200, Phillips) at an acceleration voltage of 200 KV and digital images were taken on a Gatan multipole Charge Coupled Device (CCD) camera. Energy Dispersive X-ray (EDX) analysis of the sample was carried out on an Oxford Instrument INCA attached to the FESEM. Samples for IR spectroscopy were prepared as pressed tablets of KBr or as emulsions with nujol. The spectra, recorded on a LR 64912C, Perkin Elmer infrared spectrophotometer, cover the IR region from 400 cm^{-1} to 4000 cm^{-1}. A BET surface area analyzer (SA 3100, Beckman Coulter) was used to measure nitrogen adsorption isotherm at 77 K.

6.2.4 Adsorption experiments

Standard arsenic (III) stock solution of 1000 mgL^{-1} was prepared by dissolving 1.32 g of arsenic (III) oxide in 1L volumetric flask with double distilled water. Subsequent working standard solutions were prepared from the stock by exact dilution. 100 ml of each of working arsenic(III) standard solution was taken in 250 ml conical flask and known weight of adsorbent material was added into it. The contents in the flask were shaken for 3 h on a mechanical shaker (Labtech, Daihan Labtech Ltd.) for different studies. The solution was centrifuged the mother liquor was analyzed for residual arsenic concentration by Atomic Absorption Spectroscopy. All adsorption experiments were conducted at room temperature (25 ^{o}C±0.1 ^{o}C). Batch adsorption experiments were conducted to investigate the effect of various parameters like adsorbent dose, initial concentration, presence of interfering ions, pH etc.

The specific amount of arsenic adsorbed was calculated from:

$Q_e = (C_0 - C_e) \times V/W$ ---------- (Equation 6.1)

Where Q_e is the adsorption capacity (mgg^{-1}) in the solid at equilibrium; C_0 & C_e the initial and equilibrium concentrations of arsenic (mgL^{-1}) respectively; V the volume of the aqueous solution; W is the mass (g) of adsorbent used in the experiments.[29] The effect of solution pH on arsenic removal was studied by adjusting the pH of the solution either by using 0.1 N HCl or 0.1 N NaOH. In acidic as well as basic pH, IOH NPs is stable and hence adsorption studies were carried out over the pH ranges of 2–11, which do have practical significance. The effects of the presence of diverse anions such as hydroxide, chloride, sulfate, iodide & iodate were studied at optimum experimental conditions. To study for reusability, a certain amount of arsenic from working standard solution was initially allowed to adsorb on IOH NPs at wide range of pH. After adsorption, the solid was separated by filtration and dried in air. The dried adsorbent was repeatedly subjected to the arsenic removal/adsorption experiments in order to examine the extent of reusability.

6.3 Results and Discussions

6.3.1. Analysis after characterization

X-ray diffraction (XRD) profile of nanosized iron oxide hydroxide NPs shows the presence of characteristics peaks corresponding to 2θ = 31.060, 33.100, 38.990, 41.930, 46.190, 48.210, 54.660, 57.550 and 66.380 for (310), (130), (400), (211), (301), (031), (411), (141) and (060) planes respectively and that could be indexed on the basis of orthorhombic iron oxide hydroxide (JCPDS card no. 18-0639).

The shape of iron oxide hydroxide NPs is studied by transmission electron microscopy (TEM) and is shown in Figure 6.1 It is clear that IOH NPs formed is of flower like morphology with average size of 20 nm, supporting the morphological evidence of FESEM. FESEM image in Figure 6.2(a) shows that the NPs were of flower like morphology with several strings extended and they are uniformly distributed. The micro-sized flowerlike morphology seen in FESEM image of IOH NPs (Figure 6.2) is not observed in TEM.

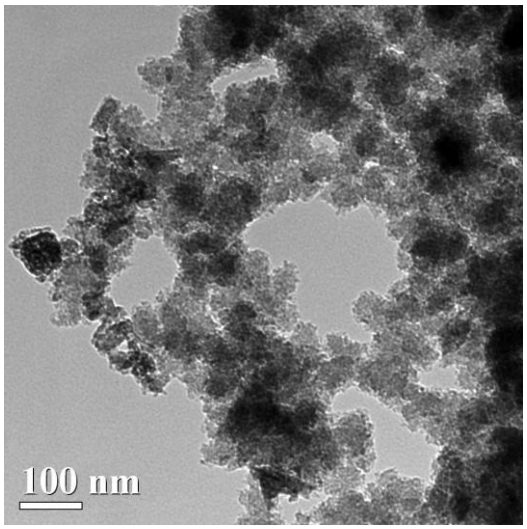

Figure 6.1(a) - TEM image of IOH NPs

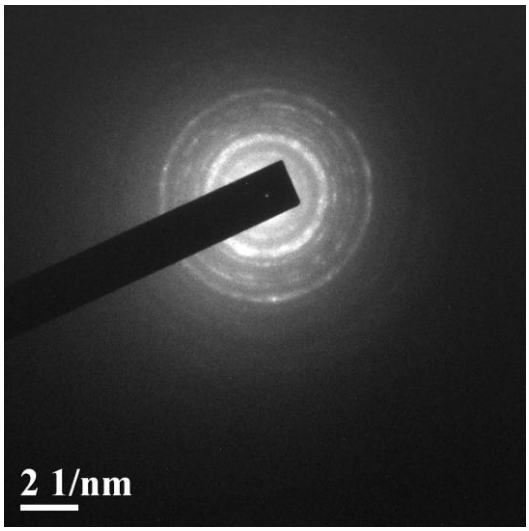

Figure 6.1(b)– SAED pattern of IOH NPs

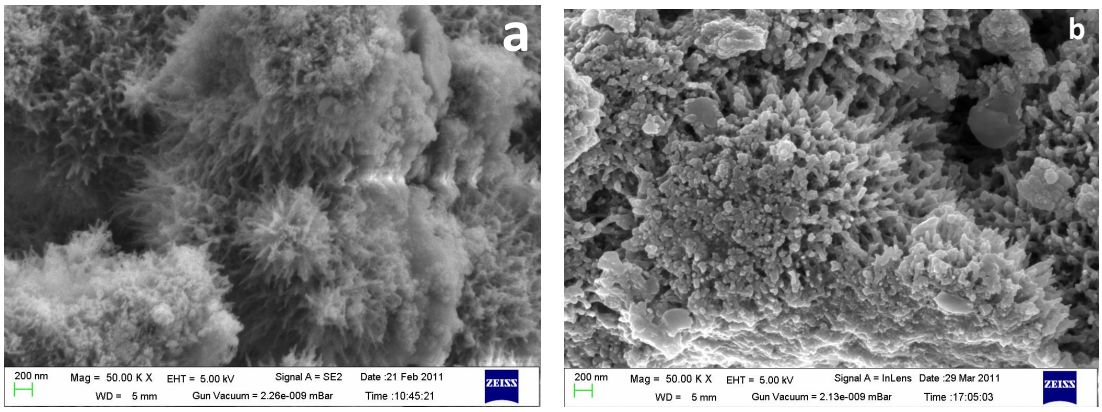

Figure 6.2 - FESEM images of IOH NPs before (a) & after (b) adsorption of arsenic

This is because of the fact that, under sonication prior to FESEM analysis leads to breakage of agglomeration of the microstructure to rather smaller entities. Such phenomenon is not unusual and also observed by Ooi *et al.* and Hassanjani-Roshan *et al.* where structure of ZnO and TiO_2 NPs are reportedly differ drastically prior and after sonication. But, in TEM analysis of IOH nano, the image has been taken prior to sonication and image of agglomerated NPs differs from flower like morphology. The surface morphologies of iron oxide hydroxide NPs before and after adsorption of arsenic(III) from water are determined by FESEM images are shown in Figures 6.2(a) and 6.2(b) respectively.

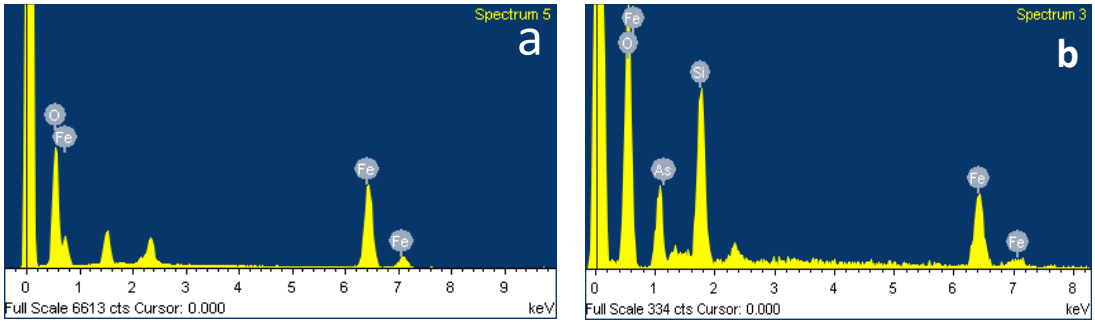

Figure 6.3 – EDX patterns of IOH nanoflower before (a) and after (b) adsorption of arsenic

Figure 6.3(a) shows only the elements of IOH NPs, whereas Figure 6.3(b) reveals the presence of arsenic including other elements of IOH nano. Thus, the adsorbent is capable to remove arsenic from water as evident from Figures 6.3(a) & 6.3(b). The specific surface area of the IOH NPs determined from BET surface area analyzer was 6.577 m^2g^{-1}.

FTIR spectroscopy is a useful tool to identify functional groups in a molecule, as each specific chemical bond often has a unique energy absorption band, and can obtain structural and bond information on a complex helps in studying the strength and type of bonding.[30] Figures 6.4(a) & 6.4(b) represent FTIR spectra of IOH nanoflower before and after treatment with arsenic respectively.

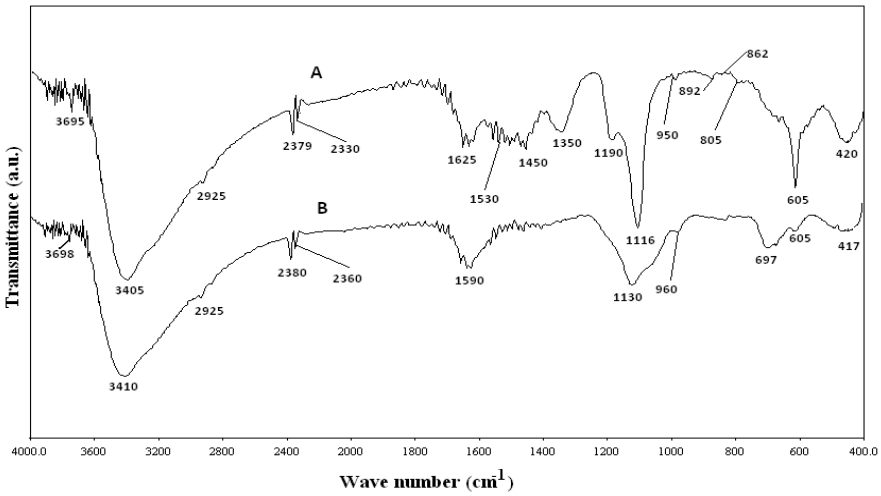

Figure 6.4 - FTIR spectra of IOH nanoflower before (a) and after (b) adsorption of arsenic

The bands at 3698 & 3410 cm^{-1} belong to the stretching vibration of hydroxyl group of IOH nanoflower as evident from Fig. 6.4(b). Fig. 6.4(a) shows that there is slight reduction in the intensity of O-H bands at 3420 cm^{-1} and appearance of a new band at 3405 cm^{-1} with some displacement to lower frequencies in arsenic treated IOH NPs which may be due to arsenic adsorption or ion exchange or both. The 605 cm^{-1} band was assigned to an asymmetric stretching vibration of As–OH groups[31] and the 805 cm^{-1} band was assigned to the stretching vibration of the As–O bond. The As–O is a shorter, stronger bond compared to that of the As–OH groups; consequently, the position of the ν(As–O) vibration(s) occurs at higher frequencies relative to their ν(As–OH) counterparts. These assignments are also supported by a recent theoretical study of the arsenite system.[32] The spectra in Fig. 4(b) clearly reveals two bands at 862 and 892 cm^{-1} which are similar to the FTIR results for arsenic adsorption on iron oxide hydroxide surface.[33] The positions of the 862 cm^{-1} and 892 cm^{-1} bands are too high in frequency to be assigned to an ν(As–OH) vibration. In an earlier IR study of arsenite sorbed to goethite, a band at 834 cm^{-1} was reported that was assigned to the ν(As–OH) of As–O–Fe groups.[34] This assignment is supported by a more recent Raman and IR study of several metal-containing arsenite salts by Myeni *et. al.* 1998.[35] In the case of As(III)/Fe oxide complex, two bands are observed with a separation of about 30 cm^{-1}. The "splitting" of the ν(As–O) vibration can be explained in two ways. First, the two vibrations correspond to the symmetric and asymmetric stretching modes of adsorbed $AsO_2(OH)_2^-$ complex. The separation between the symmetric and asymmetric vibrations, however, is larger than the splitting in aqueous solution. Furthermore, in aqueous solution the asymmetric ν(As–OH) vibration (high-frequency band) is observed to have more intensity than the symmetric ν(As–OH) vibration. The opposite behavior is observed here. The second interpretation of the spectral data is that there are two distinct types of As–O groups. The 862 cm^{-1} band would be assigned the Fe–O–As groups and the 892 cm^{-1} band would correspond to non-surface-complexed As–O bonds of the adsorbed As(V) species. The band within 1300-1500 cm^{-1} indicates the bending vibration of O-H group of complexed as well as free molecules.

6.3.2 Zero point charge (ZPC) determination

The zero point charge (ZPC) is a good tool to determine the surface charge of the materials and ultimately adsorption of the specific adsorbate on adsorbent depends

on the surface charge of adsorbent. The zero point charge of any materials describes the condition when the electrical charge density on a surface is zero[36] and at that condition there is mere probability of occurring adsorption through ion-exchange process. pH of solution after adsorption *vs* pH before adsorption is plotted and shown in Figure 6.5. The horizontal portion of the graph parallel to the X-axis indicates ZPC of material. The ZPC value of IOH NPs is found to be 3.38. In experimental condition (pH 6.2, Temp. 25 ^{0}C) pH is greater than 3.38, so the NPs are positively charged. "The adsorbent surface has a strong positive charge (cationic) under our experimental condition".

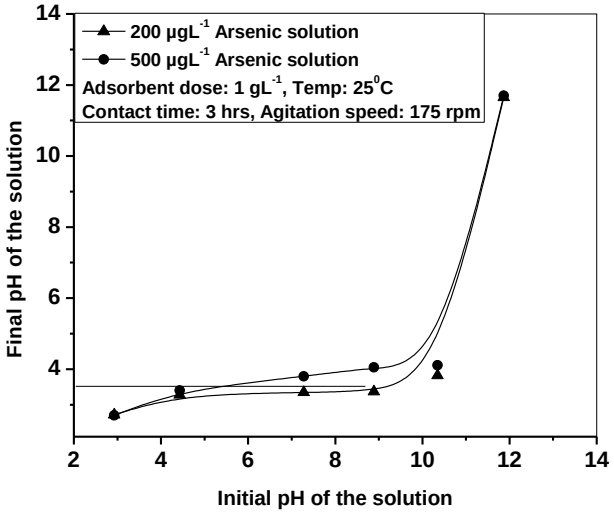

Figure 6.5: Plot of final pH *vs* Initial pH

6.3.3 Effect of contact time

Figure 6.6 indicates the effect of contact time on the adsorption capacity and here it is followed that the rapid adsorption of arsenic took place within 90 min. Subsequently, adsorption became slow and almost reached to equilibrium within 180 min. With further increase in contact time upto 9 h, no appreciable removal of arsenic takes place, indicating that complete adsorption occurred within 3 h. Thus, subsequent adsorption experiments were conducted for a period of 3 h.

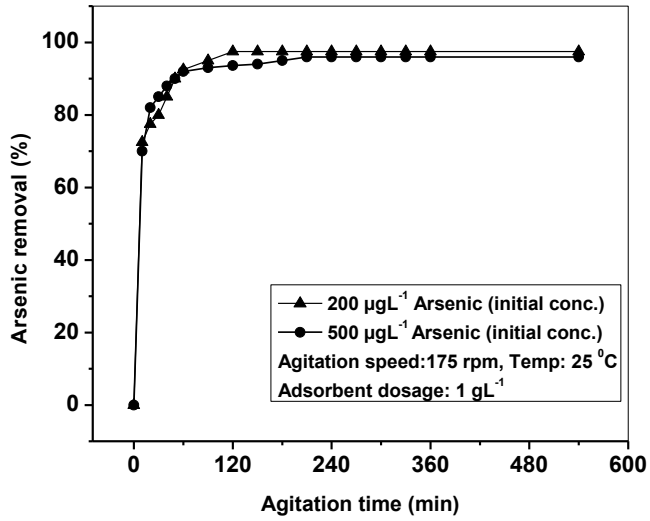

Figure 6.6: Plot of arsenic removal (%) *vs* Agitation time

6.3.4 Effect of sorbent dosage

To optimize the minimum dosage required for bringing down the arsenic level to the tolerance limit, dosages of sorbent (0.1–4 gL^{-1}) was varied. The percentage removal of arsenic with different adsorbent dosage is shown in Figure 6.7. The IOH NPs was found to be efficient for removal arsenic from 200 μgL^{-1} and 500 μgL^{-1} to 3 μgL^{-1} & 25 μgL^{-1} respectively with 1 gL^{-1} dosage. The percentage removal of arsenic significantly increased with sorbent dosage, which was obvious because of the increase in the number of active sites as the dosage increases.[37]

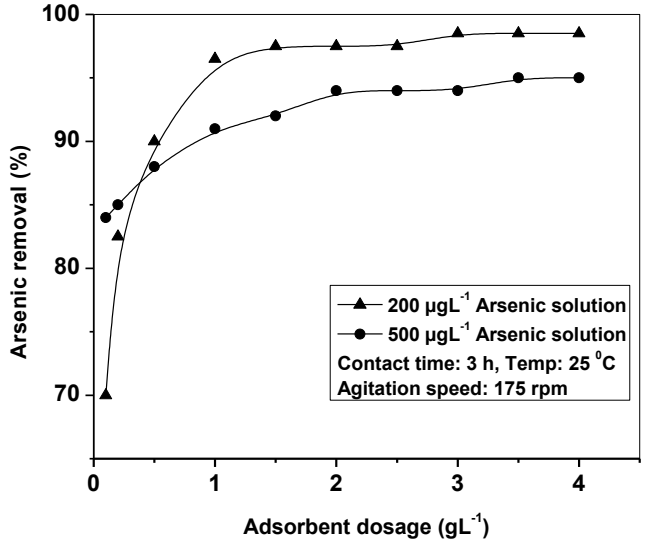

Figure 6.7: Plot of Arsenic removal (%) *vs* adsorbent dose

Hence, in all the subsequent experiments 1.0 gL^{-1} of adsorbent was fixed as the optimum dosage, to give reasonable dearsenification efficiency.

6.3.5 Effect of initial concentration

For the initial concentration of working As(III) solutions upto 1000 μgL^{-1} & adsorbent dosage 1 gL^{-1}, more than 92% removal was observed within 3 h contact time. It was evident that for lower initial concentrations of arsenic, the adsorption was very fast. The removal of arsenic decreased with increase in initial concentration and took longer time to reach equilibrium. With increase in arsenic concentration, competition for the active adsorption sites increased and the adsorption process was gradually slowed down. The percentage of arsenic removal versus initial concentration was shown in Figure 6.8.

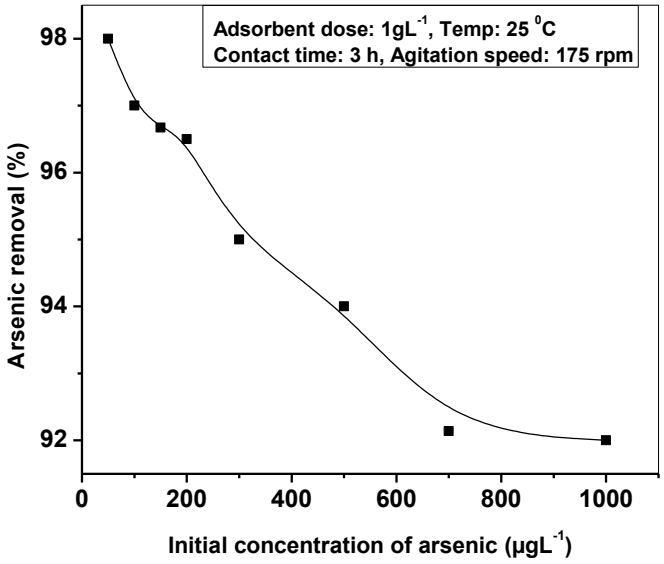

Figure 6.8: Effect of initial arsenic concentration on arsenic removal

6.3.6 Influence of pH & mechanism of sorption

The effect of pH on the efficiency of sorbent was studied at different pH from 2 to 11 keeping other parameters constant as shown in Figure 6.9. The arsenic removal was found more than 95% at pH 7-8 whereas, it was less than 85% at acidic pH. This result clearly showed that removal percentage of arsenic was slightly higher in basic pH compared to acidic one. The variation in uptake with respect to the initial solution

pH can be explained on the basis of ZPC of the adsorbent. The maximum sorption capacity of the sorbent is found to be 475 $\mu g g^{-1}$ for As(III) at 25 ^{o}C and at pH 7.28.

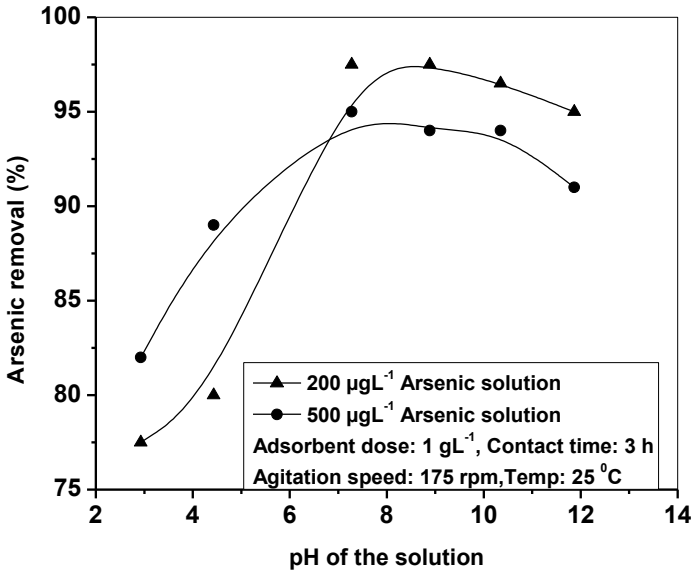

Figure 6.9: Effect of pH on the percentage adsorption of arsenic

To understand the arsenic adsorption behavior under different pH values, the following reactions are considered.[6] The iron oxide hydroxide NPs surface contains several hydroxide groups which were protonated above the zeta potential pH. According to Grossl *et al.,* 1997 the mechanism for oxyanion adsorption on iron oxide hydroxide materials is a two-step process resulting in the formation of an inner-sphere bidentate surface complex and shown in Figure 6.10.

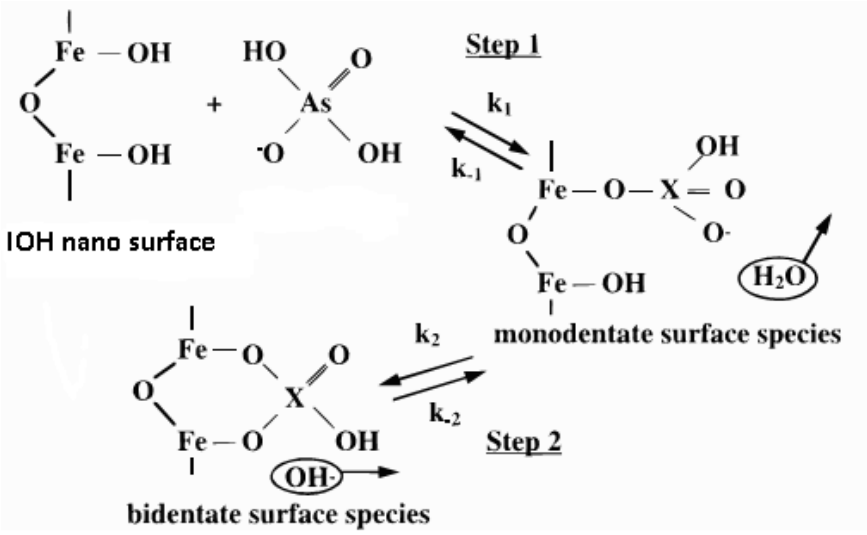

Figure 6.10: Plausible mechanism of arsenic adsorption

The first step involves an initial ligand exchange reaction of the aqueous oxyanion ($H_2AsO_3^-$) with iron oxide hydroxide, forming an inner-sphere monodentate surface complex. The rate constant of first step was fast compared to second step as formation of bidentate ligand leads to decrease of entropy of the system. The succeeding step involves a second ligand exchange reaction, resulting in the formation of an inner-sphere bidentate surface complex. At acidic pH the IOH nanoflower was almost neutral, so the adsorption of arsenic was not favourable upto the mark. The arsenic adsorption decreased sharply at basic pH (>9) due to increased repulsive forces between the negatively charged arsenite ions and the IOH nano. Below pH 9 of the solution, As(III) remains as neutral species like $HAsO_2$, H_3AsO_3 or other species, so repulsive forces between As(III) and IOH nano is not active. But at pH> 9.2 the As(III) becomes charged species like $HAsO_3^{2-}$, H_2AsO_3 and being repelled to some extent by Iron Oxide Hydroxide NPs during adsorption. The charged species formation above pH>9.2 is also supported by some books on Arsenic.[38,39] Thus the mechanism of arsenic removal of IOH NPs follows both adsorption and ion-exchange mechanism.

6.3.7 Effect of agitation speed of mechanical shaker on adsorption

Stirring is an important parameter in adsorption studies influencing the distribution of the solute in the bulk solution and the formation of the external boundary layer.[40] Figure 6.11 showed the percentage removal of arsenic using IOH NPs at five different stirring speeds viz. 125, 150, 175, 200 and 225 rpm. It is clear that stirring speed does not have any appreciable influence on the adsorption of different concentration of arsenic by IOH nano materials. However, optimal removal efficiency was obtained at 175 rpm, so whole experiment was carried out at that shaking speed. This was due to the fact that the solid was completely and homogenously suspended at the stirring speed higher than 110 rpm. In such cases stirring speed had no significant effect on adsorption rate.[41] Hence, it is proposed that external diffusion is not the limiting step in this adsorption process.

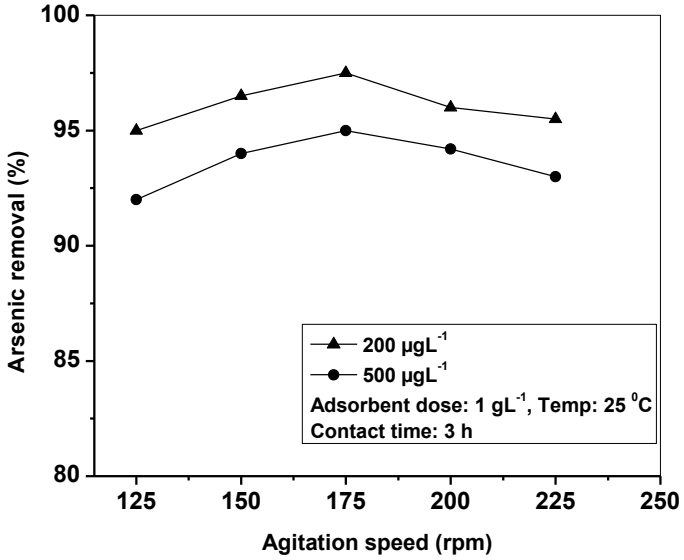

Figure 6.11: Effect of agitation speed on removal of arsenic

6.3.8 Influence of competing anions

The contaminated drinking water may contain several common other anions, viz., OH^-, SO_4^{2-}, PO_4^{3-} etc. which can compete with the arsenic during sorption process. Hence the adsorption was studied in the presence of diverse anions with varying initial concentrations of these ions viz., 0.2, 0.5, 1.0 & 1.5 mM keeping the initial arsenic concentration of 200 μgL^{-1} and 500 μgL^{-1} at 25 ^oC. Figure 6.12 shows the efficiency of removal capacity of arsenic by IOH NPs in the presence of other competing anions at double distilled water pH (pH~ 5.90).

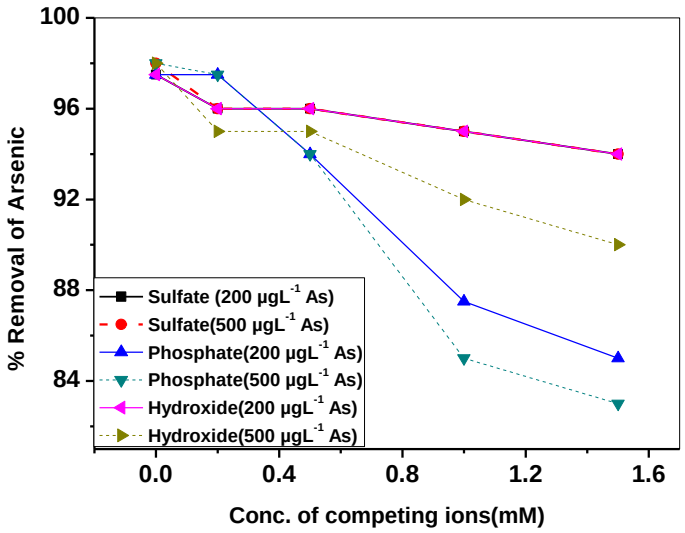

Figure 6.12: Effect of competing anions on removal of arsenic

Other conditions of the adsorption studies being kept constant e.g. agitation speed 175 rpm, temperature 25 ^{0}C and contact time of 3 hrs. With the increase in the concentration of these anions, efficacy of IOH nanoflower towards removal of arsenic from water was observed. It may be due to a competition among them for the sites on the sorbent surfaces, which in turn is decided by the concentration, charge and size of the anions. The presence of competing anions like phosphate ion has a significant effect on arsenic adsorption by IOH NPs followed by hydroxide and sulphate ion respectively.[42]

The percentage of arsenic removal decreased sharply after 0.5 μgL^{-1} concentration of competing ions and the trend was followed in case of both 200 μgL^{-1} as well as 500 μgL^{-1} concentration of arsenic. The concentrations of competing anions in this study were far higher than those likely to be encountered in groundwater. Thus, IOH NPs was able to remove arsenic from water over a broad range of pH in presence all interfering ions except high concentration of phosphate ion. In presence hydroxide at higher concentration, pH of the solution is slightly increased and in that condtion experiment on competing ion effect has been performed. It was seen that there was no competing ion effect on adsorption of arsenic by IOH NPs. The same trends were also followed by other ions like sulfate and phosphate ion.

6.4 Adsorption Kinetics

The rate of adsorption was determined by studying the adsorption kinetics at two different initial arsenic concentrations of 200 μgL^{-1} and 500 μgL^{-1} at optimum adsorbent dose. It was observed that arsenic removal increased with the lapse of time and the rate was initially rapid, after which the rate slowed down as the equilibrium approached. For evaluating the adsorption kinetic two models are employed, the pseudo-first order[43] and the pseudo-second order models.[44] The pseudo-first order kinetic equation is expressed as:

$$q_t = q_e - \exp\left(ln\, q_e - k_1 t\right)$$ ---------- (Equation 6.2)

Where, (min^{-1}) is the rate constant of pseudo-first order adsorption, q_e and q_t (mg/g) are the adsorbed amount at equilibrium and at time t.

The pseudo-second order rate equation is expressed as:

$$q_t = \frac{q_e^2 k_2 t}{1+q_e k_2 t}$$ ---------- (Equation 6.3)

Where k_2 is the rate constant of pseudo-second order model (g/mg /min).

The non-linear plot of pseudo-first order and pseudo-second order for sorption of arsenic onto adsorbent are presented in Figures 6.13 and 6.14 respectively. The parameters of the kinetic models fits and their corresponding chi square and RMSE values are given in Table 6.1. As seen from the Table, the value of Chi square statistic and RMSE value of pseudo-second order models are lower than the corresponding pseudo-first order model which suggests that the present system follows pseudo-second order kinetic.

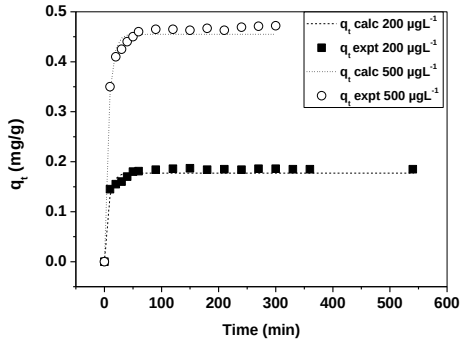

Figure 6.13: K_1 kinetics, pseudo-first order plots

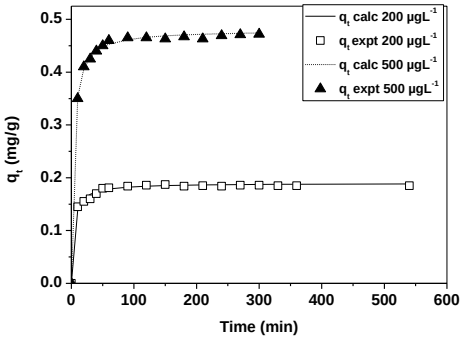

Figure 6.14:- K_2 kinetics, pseudo-second order plots

Table 6.1 - Pseudo-first order and pseudo-second order kinetic parameters for two different initial arsenic concentrations (C_0).

C_0	Pseudo-first order				Pseudo-second order			
(mg/L)	k_1 (min^{-1})	q_e (mg/g)	χ^2	RMSE	K_2 (min^{-1})	q_e (mg/g)	χ^2	RMSE
0.200	0.1390	0.1772	0.0074	0.0091	1.4218	0.1897	0.0014	0.0039
0.500	0.1372	0.4548	0.0052	0.1391	0.5774	0.4800	0.0006	0.0046

6.4.1 Intraparticle diffusion

The intraparticle diffusion model has often been used to determine if intraparticle diffusion is the rate-limiting step. The existence of intraparticle diffusion process can be determined from the following equation.[45,46]

$q_t = k_i t^{0.5}$ ---------- (Equation 6.4)

Where, k_i is the intraparticle diffusion rate constant (mg/g $min^{-0.5}$). If intra-particle diffusion is a rate-limiting step, then the plot should be linear and pass through

the origin. Figure 6.15 shows that the plot is multilinear over the whole time range suggesting that adsorption occurred in three phases. The initial steeper section represents surface or film diffusion, the second linear section represents a gradual adsorption stage where intraparticle or pore diffusion is rate-limiting and the third section is finial equilibrium stage. Therefore, the adsorption of arsenic onto IOH nanoflower is both surface adsorption as well as intraparticle diffusion effect.

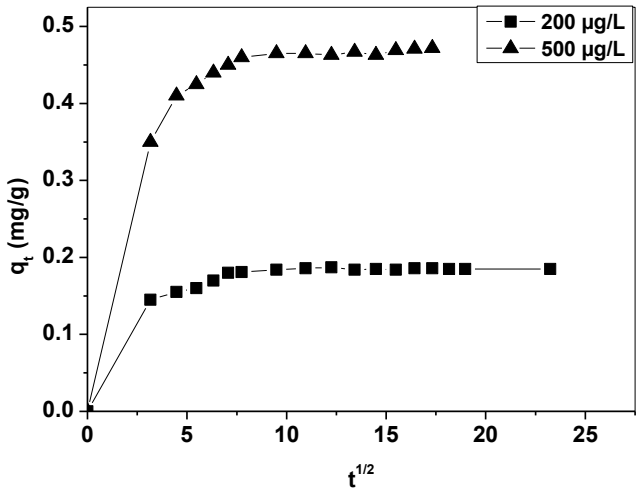

Figure 6.15: The amount of arsenic adsorbed (q_t) *vs* the square root of time ($t^{0.5}$)

6.5 Adsorption isotherms

The adsorption isotherms are generally used to describe how adsorbate interacts with adsorbent at equilibrium and therefore it is critical in optimising the use of adsorbents. Five different isotherms have been adopted to understand the mechanism of adsorption for the removal of arsenic. Theoretical plots of each isotherm were tested for their correlation with the experimental results. Figure 5.16 shows the comparison of different isotherms studied at 25 ^{o}C.

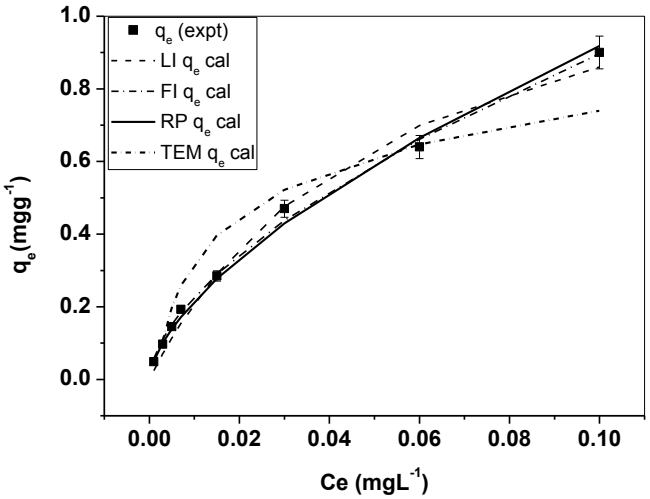

Figure 6.16: Equilibrium isotherm model for arsenic adsorption

6.5.1 Langmuir Isotherm

The Langmuir adsorption isotherm (Langmuir 1918) is given by

$$q_e = \frac{q_m b C_e}{1+bC_e}$$ ---------- (Equation 6.5)

Where, q_e is the equilibrium quantity adsorbed (mgg^{-1}), qm is the maximum capacity of monomer adsorption (mgg^{-1}), C_e the equilibrium concentration (mgL^{-1}), b the adsorption equilibrium constant (Lmg^{-1}) related to the energy of adsorption. The Langmuir equation is valid for monolayer sorption onto a surface with a finite number of identical sites.[47] The experimental adsorption data and the values of the isotherm parameters calculated non-linearly are given in Table 6.2.

In order to predict the adsorption efficiency of the adsorption process the essential characteristics of the Langmuir isotherm can be determined in terms of dimensionless equilibrium parameter or Langmuir isotherm constant parameter (R_L) which can be related with b by the following equation.[48]

$$R_L = \frac{1}{1+bC_o}$$ ----------(Equation 6.6)

Where is the initial arsenic ion concentration (mgL^{-1}). The value of indicates the shape of the isotherms. If the value $is\ 0 < R_L < 1$ then the Langmuir isotherm is favorable. When $R_L = 0$ it is irreversible and $R_L = 1$, it is linear whereas isotherm is unfavourable with the value, $R_L > 1$. R_L at initial concentration is found to be 0.5131.

Table 6.2 - Characteristic parameters of different Isotherm models for the adsorption of arsenic by Iron Oxide Hydroxide nanoflower

Isotherm	Parameters	Value
Langmuir	R^2	0.9942
	q_m (mg/g)	1.31
	b (L/mg)	18.98
	X^2	0.0580
	RMSE	0.0386
	R_L	0.5131
Freundlich	R^2	0.9934
	K_f ($mg^{1-1/n}$ $L^{1/n}$ g^{-1})	3.52
	1/n	0.5944
	X^2	0.0071
	RMSE	0.0179
Redlich-Peterson	R^2	0.9950
	A	2.75E+05
	B (L/mg)	7.03E+04
	G	0.3701
	X^2	0.0082
	RMSE	0.0186
Temkin	R^2	0.9408
	A_t	600.68
	B_T	13.72
	X^2	0.1040
	RMSE	0.0872

6.5.2. Freundlich Isotherm

The Freundlich isotherm is employed to model the multilayer adsorption based on sorption onto heterogeneous surface[49] and is given by

$$q_e = K_f C_e^{1/n} \quad \text{---------- (Equation 6.7)}$$

Where, ($mg^{1-1/n}L^{1/n}g^{-1}$) is Freundlich constant indicative of the relative adsorption capacity of the adsorbent and n is the empirical parameter representing adsorption intensity of the adsorbent. The values of and n calculated non-linearly are given in Table 6.2. The magnitude of the exponent n gives an indication on the favorability of arsenic adsorption.[50] The conditions are found to be favorable as the value of 1/n lies between 0 and 1 and the value of 'n' is greater than 1. A plot of the experimental data and non-linear form is shown in Figure 6.16.

6.5.3 Redlich–Peterson Isotherm

The Redlich–Peterson isotherm contains three parameters and is a special case model that incorporated the features of the Langmuir and Freunlich isotherms into a single equation and presents general isotherms equation.[51] It can be described as follows:

$$q_e = \frac{A C_e}{1 + B C_e^g} \quad \text{---------- (Equation 6.8)}$$

Where A: Redlich–Peterson constant (Lg^{-1}); B: affinity coefficient (L mg^{-1} As); g (0 <g<1) heterogeneity coefficient, q_e: uptake at equilibrium (mgg^{-1} As), C_e: equilibrium concentration (mgL^{-1} As). The calculated g value was found to be 0.37 and indicating the heterogeneity of the adsorbent surface. This is also supported by RMSE value and χ^2 values respectively.

6.5.4 Temkin Isotherm

The Temkin isotherm model assumes that the adsorption energy decreases linearly with the surface coverage due to adsorbent–adsorbate interactions. The derivation of the Temkin isotherm assumes that the fall in the heat of sorption is linear rather than logarithmic, as implied in the Temkin equation.[52] The Temkin equation is given as below:

$$q_e = \frac{RT}{B_T} \ln (A_T C_e) \text{ ---------- (Equation 6.9)}$$

Where, A_T is the equilibrium binding constant, (L mg^{-1}), b_T is the Temkin constant related to the variation of adsorption energy (kJ mol^{-1}).[53] Values of A_T and B_T are presented in Table 6.2. The variation of adsorption energy shows a positive value indicating that the reaction is exothermic in nature.[54]

6.6 Arsenic desorption study

The exhausted IOH NPs were regenerated with eluents like dilute HCl and dilute NaOH.[55] Desorption efficiency of IOH NPs was studied using 0.2M & 0.5M HCl and 0.2M & 0.5M NaOH as eluents and all the regeneration experiments were carried out at room temperature. From Table 6.3, it is evident that out of the two eluents, NaOH had been identified as the best eluent as it had 75% desorption efficiency whereas HCl showed a maximum of 54% desorption efficiency.

Table 6.3 - Regeneration study (adsorbent dosage: 1 gL^{-1})

Initial conc. of As(III) (μgL^{-1})	Eluent used	Conc. of eluent (M)	Conc. of As(III) in eluent after treatment (μgL^{-1})	Regeneracy of adsorbent (%)
200	NaOH	0.2	90	45
200	NaOH	0.5	140	70
200	HCl	0.2	60	30
200	HCl	0.5	100	50
500	NaOH	0.2	270	54
500	NaOH	0.5	375	75
500	HCl	0.2	160	32
500	HCl	0.5	270	54

6.7 Conclusions

Iron oxide-hydroxide NPs has been found to be a potential adsorbent for the removal of arsenic from water with a maximum sorption capacity of 475 μgg^{-1} for arsenic at room temperature. The sorption of arsenic onto iron oxide NPs is significantly influenced by pH of the medium. Equilibrium sorption data fit better to Redlich-Peterson followed by Langmuir, Freundlich and Temkin sorption models respectively. Thus the sorption shows heterogeneity of the adsorbent surface. Study on adsorption kinetics shows that the present system follows pseudo-second order kinetic. The mechanism of arsenic removal of iron oxide-hydroxide NPs follows both ion-exchange and adsorption process which is mainly due to physical adsorption and the variation of adsorption energy shows that it is exothermic in nature. There is no significant influence of other co-anions like hydroxide, sulphate and phosphate ions on the dearsenification capacity of the NPs except high concentration of phosphate ions. The adsorped material can be regenerated up to 75% by using dilute acid as well as alkali. It is expected, that the present research work may provide new dimensions in developing iron oxide NPs through a simple approach, which can be scaled up and further explored as an effective and replicable adsorbent media for dearsenification of drinking water.

References:

1. Tanaka, T. *Appl. Organometal. Chem*. **2** (4), 283--295, 1988.
2. Huang, S.Y., et al. *British J. Haematol*. **103** (4), 1092--1095, 1998.
3. Igor, R.A., et al. *Arsenic adsorption in soils with different mineralogical compositions. INCT-ACQUA – Annual Report*, Institute of Science and Technology for Mineral Resource, Water and Biodiversity, 2010.
4. Webb, S.M., et al. *Environ. Sci. Tech*. **37** (4), 754--760, 2003.
5. Manning, B.A. & Goldberg, S. *Environ. Sci. Tech*. **31** (7), 2005--2011, 1997.
6. Grossl, P.R., et al. *Environ. Sci. Tech*. **31** (2), 321--326, 1997.
7. Thirunavukkarasu, O.S., et al. *Water Qual. Res. J. of Canada* **36** (1), 55--70, 2001.
8. Johnston, R., et al. *Safe Water Technology for Arsenic Removal*, Chapter 6, 2001.
9. Ahmed, M. & Rahman, M.M. *Water Supply and Sanitation - Rural and Low-Income Urban Communities,* ITN-Bangladesh Centre for Water Supply and Waste Management, Dhaka, Bangladesh. 2000.
10. Bajpai, S. & Chaudhuri, M. *J. of Environ. Eng.* **125** (8), 782--784, 1999.
11. Acharyya, S.K., et al. *Environ. Geology* **52** (3), 489--501, 2007.
12. Manning, B.A., et al. *Environ. Sci. Tech*. **36** (5), 976--981, 2002.
13. Cherry, J.A., et al. *J. Hydrology* **43** (1-4), 373--392, 1979.
14. Sadiq, M., et al. *Water Air Soil Poll*. **20** (4), 369--377, 1983.
15. Masscheleyn, P.H., et al. *J. Environ. Qual*. **20**, 522--527, 1991.
16. Ferguson, J.F., et al. *Water Res*. **6** (11), 1259--1274, 1972.
17. Korte, N.E., & Fernando, Q. *Crit. Rev. in Environ. Contr.* **21** (1), 1--39, 1991.
18. Gulens, J., et al. *Influence on redox environments on the mobility of arsenic in ground water (Chapter 4). In: Rubia, A. J., Ed.; Chemistry of Water Supply Treatment and Distribution,* Ann Arbor Science Publishers: Ann Arbor, MI, 1973.
19. Yu, X.Y., et al. *J. Phys. Chem. C* **115** (45), 22242--22250, 2011.
20. Yu, X.Y., et al. *Nanoscale* **4** (11), 3466--3474, 2012.
21. Yu, X.Y., et al. *ACS Appl. Mater. Interfaces* **4** (4), 1954--1962, 2012.
22. Jia, Y., et al. *Dalton Trans.* **42** (5), 1921--1928, 2013.
23. Zhu, B.J., et al. *J. Phys. Chem. C* **116** (15), 8601--8607, 2012.
24. Peng, F., et al. *Mater. Res. Bull*. **48** (6), 2180--2185, 2013.
25. Raul, P.K., et al. *J. Nanosci. Nanotech.* **12** (5), 3922--3930, 2012.

26. Adegoke, H.I., et al. *Poly. J. Environ. Studies* **22**(1), 7--24, 2013.
27. Fendorf, S., et al. *Environ. Sci. Tech.* **32**(2), 315--320, 1997.
28. Ding, M., et al. *Geochim Cosmochim. Acta.* **64** (7), 1209--1219, 2006.
29. Abdelwahab, O. *Egyptian J. Aqua. Res.* **33** (1), 125--143, 2007.
30. Li, N., et al. *Ind. Eng. Chemical Res*. **44**, 6692--6700, 2005.
31. Loehr, T.M., et al. *Inorg. Chem*. **7**, 1708--1714, 1968.
32. Tossell, J.A. *Geochimica et Cosmochimica Acta* **61** (8), 1613--1623, 1997.
33. Suarez, D.L., et al. *ACS Symposium Series* **715**, 136--178, 1998.
34. Lumsdon, D.G., et al. *J. Soil Sci*. **35**(3), 381--386, 1984.
35. Myneni, S.C.B., et al. *Geochimica et Cosmochimica Acta*, **62**(19), 3285--3300, 1998.
36. Russel, W.B., et al. *A book on Colloidal Dispersions*, *Cambridge* University Press, Cambridge, 1989.
37. Mellah, S., & Chegrouche, S. *Water Res*. **31**(3), 621--629, 1997.
38. Henke, K., *Arsenic: Environmental Chemistry, Health Threats and Waste Treatment*, John Wiley & Sons, 2009.
39. Welch, A.H., et al. *Arsenic in Ground Water: Geochemistry and Occurrence*, vol. XI, 47, Springer publishers, 2003.
40. Darmadia, C., et al. *Asean J. Chemical Eng*. **8**(1), 27--38, 2008.
41. Rodrı´guez, A., et al. *Indust. Eng. Chem. Res*. **49**(7), 3207--3216, 2010.
42. Guan, X., et al. *Water Res.* **43**(15), 3891--3899, 2009.
43. Lagergren, S. *Vetenskapsakad. Handl*. **24** (4), 1--39, 1898.
44. Ho, Y.S., et al. *Water Res*. **34**(3), 735--742, 2000.
45. Namasivayam, C., et al. *Environ. Poll*. **89**(1), 1--7, 1995.
46. Boparai, H.K., et al. *J. Hazard. Mater.* **186**, 458--465, 2011.
47. Parimal, S., et al. *Ind. Eng. Chem. Res*. **49** (6), 2882--2888, 2010.
48. Hall, K.R., et al. *Ind. Eng. Chem. Fund.* **5**(1), 212--223, 1966.
49. Freundlich, H.M F. *J. Phys. Chem*. **57**(A), 385--470, 1906.
50. Treybal, R.E. *Mass transfer equations*, 3rd Ed., Mc Graw-Hill, New York, 1981.
51. Redlich, O., & Peterson, D.L. *J. Phys. Chem*. **63**(6), 1024--1024, 1959.
52. Temkin, M.J. & Pyzhev, V. *Acta Physiochim*. *URSS* **12**(1), 217--222, 1940.
53. Elebi, O.C., et al. *J. Hazard. Mat.* **148**(3), 761--767, 2007.
54. Hadi, M., et al. *Chem. Eng. J.* **160**(2), 408-416, 2010.
55. Viswanathan, N., et al. *J. Hazard. Mater*. **161**(1), 423--430, 2009.

56. Woman carrying water image in front page: https://encrypted-tbn3.gstatic.com/images?q=tbn:ANd9GcQUiUgbushfaf37MOTo2z7lyy0MC-GNmvAfJi5X-_aZCrXFup-G2 Q
57. Arsenic poisoning image in front page: http://www.bioearthinc.com/leg.gif
58. Glass water image in front page: https://encrypted-tbn3.gstatic.com/images?q=tbn:ANd9GcQlM6fvL3oKf741y-3QGN4Ofs84TugRm5O9zQg6EgYbHcr3jUiiBQ